PASJ: Publ. Astron. Soc. Japan **59**, S857–S864, 2007 November 30

EUV Emission Lines and Diagnostics Observed with Hinode/EIS

Peter R. YOUNG,[1] Giulio DEL ZANNA,[2] Helen E. MASON,[3] Ken P. DERE,[4] Enrico LANDI,[5]
Massimo LANDINI,[6] George A. DOSCHEK,[7] Charles M. BROWN,[7] Len CULHANE,[2]
Louise K. HARRA,[2] Tetsuya WATANABE,[8] and Hirohisa HARA[8]
[1]*STFC Rutherford Appleton Laboratory, Chilton, Didcot, Oxfordshire, OX11 0QX, UK*
[2]*University College London, Department of Space and Climate Physics, Holmbury St. Mary, Dorking, Surrey, UK*
[3]*DAMTP, Centre for Mathematical Sciences, Wilberforce Road, Cambridge CB3 0WA, UK*
[4]*George Mason University, 4400 University Dr., Fairfax, VA 22030, USA*
[5]*Artep, Inc at Naval Research Laboratory, 4555 Overlook Ave. S.W., Washington D.C. 20375-5320, USA*
[6]*Dipartimento di Astronomia e Scienza dello Spazio, Universitá di Firenze, Largo E. Fermi 2, 50125 Florence, Italy*
[7]*Code 7670, Naval Research Laboratory, Washington, D.C. 20375-5352, USA*
[8]*National Astronomical Observatory of Japan, 2-21-1 Osawa, Mitaka, Tokyo 181-8588*

(Received 2007 June 12; accepted 2007 August 14)

Abstract

Quiet Sun and active region spectra from the Hinode/EIS instrument are presented, and the strongest lines from different temperature regions discussed. A list of emission lines recommended to be included in EIS observation studies is presented based on analysis of blending and diagnostic potential using the CHIANTI atomic database. In addition we identify the most useful density diagnostics from the ions covered by EIS.

Key words: line: identification — Sun: corona — Sun: transition region — Sun: UV radiation

1. Introduction

The EUV Imaging Spectrometer (EIS) on board Hinode (Kosugi et al. 2007) takes high resolution spectra in the two wavelength bands 170–211 Å and 246–292 Å, referred to here as the short and long wavelength bands (SW and LW, respectively). The instrument is described in detail by Culhane et al. (2007). The two wavelength bands were chosen as they contain excellent diagnostics of coronal and flaring plasma; the SW band in particular is the most rich in coronal plasma diagnostics in the whole EUV region, and EIS is the first satellite-based instrument to observe it in high resolution.

Constraints due to on board storage and telemetry mean that for EIS observations with a reasonable cadence and spatial coverage it is not possible to send the complete spectra to Earth. An on board selection of particular emission lines is thus performed, the reduced telemetry consisting of a set of windows w pixels wide by h pixels high centred on each of the selected wavelengths. The most important aspect of designing an EIS observation study is to choose the emission lines for the science you want to do. The present paper provides a guide to the most prominent and useful emission lines in the EIS spectra based on early data analysis, and also highlights key density diagnostics. Pre-flight descriptions of the EIS capabilities, including diagnostics and line identifications, are given in Del Zanna and Mason (2005a).

2. Instrument Capability

The EIS instrument is performing very well in terms of expected sensitivity and spectral resolution, and the observed spectra are very similar to pre-flight predictions made by Del Zanna and Mason (2005a) using the CHIANTI database (Landi et al. 2006; Dere et al. 1997) and the expected instrument parameters. Figures 1 and 2 show sample averaged spectra obtained with EIS for quiet and active regions observed on 2006 December 23, 16:10 UT and 2006 November 4, 11:49 UT, respectively. The 1″ slit was used in each case. The full width at half maximum of the emission lines is around 0.065–0.075 Å (3–3.5 pixels), corresponding to a spectral resolution of $\approx$ 3000–4000.

A key factor when judging the usefulness of an EIS emission line is the telescope effective area (EA) at that wavelength, which determines the fraction of incident photons that arrive at the detector. The EA curves are overplotted as dashed lines on the spectra in figures 1 and 2. The use of two different multilayer coatings on the EIS optical surfaces leads to EA curves that are peaked for the two bands, with less sensitivity at the ends of each wavelength range. This is particularly so for the SW band which peaks at 196 Å, very close to the strong λ195.12 line of Fe XII, making this the strongest line observed by EIS in most conditions. The Fe IX λ171.07 and Fe X λ174.53 lines are comparable in strength to Fe XII λ195.12 in moderately active solar conditions (Malinovsky & Heroux 1973), but when observed with EIS they are factors 1000 and 200 times weaker than λ195.12, respectively. The EA curve for the long wavelength (LW) band is less peaked giving a more consistent instrument sensitivity across the band. The shape of these EA curves is an important consideration when choosing emission lines for EIS observation studies: a weak line near 195 Å can yield more instrument counts than a stronger line at the edges of the EA curve. Specific examples of this are discussed below.

Another important factor when considering emission lines is the degree of blending. Even with the high spectral resolution of EIS, many lines are blended with other species, particularly

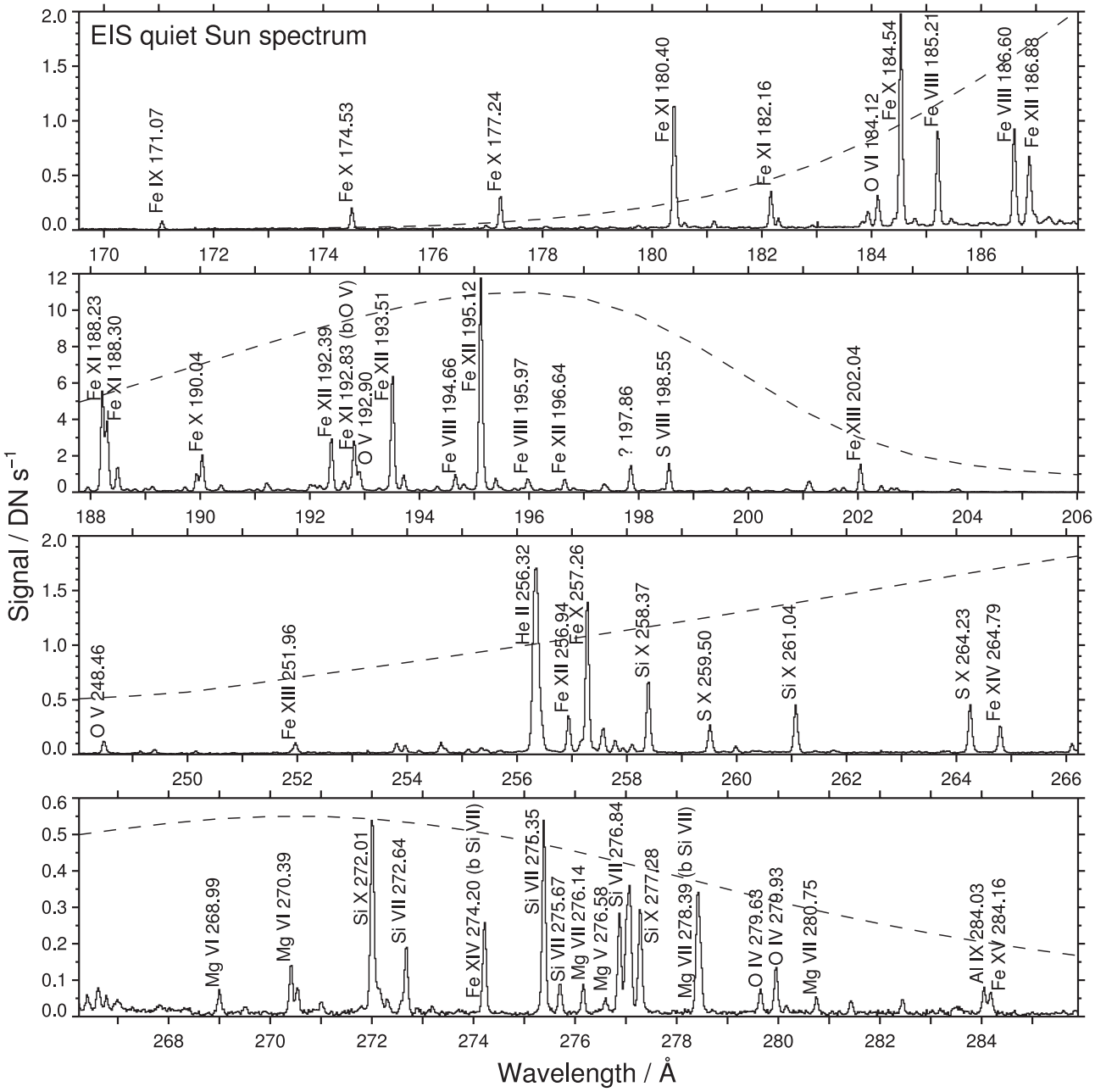

Fig. 1. EIS quiet Sun spectrum obtained on 2006 December 23 with identifications of important lines shown. The dashed line shows the effective area of the instrument, which has a peak value of 0.31 cm^2 in the SW band and 0.11 cm^2 in the LW band.

in the SW band. Examples of such blends are described below and include the blending of two of the three EIS "core lines" — He II λ256.32 and Ca XVII λ192.82 — which are lines included by default in all EIS observation studies. In many cases the contributions of blending lines can be estimated quite accurately by making use of line ratios that are insensitive to the plasma conditions and again examples are given below.

The ions discussed in the following sections we believe will be sufficient for most science studies. However, there are a number of interesting lines from ions of nickel, sulphur, argon, and calcium that will be valuable for abundance or flare studies. Discussion of these lines will be deferred to a future paper.

All atomic data used in compiling this paper are from v.5.2 of the CHIANTI atomic database (Landi et al. 2006; Dere et al. 1997) and, in particular, all wavelengths given below are from CHIANTI. When referring to intensity ratios below, ratios in energy units (rather than photon units) are implied. When referring to the strength of EIS lines, we usually use the measure "data number" (DN), which is the unit for the data stored in the level 0 EIS FITS files. The number of photons is obtained by multiplying the DN by a wavelength varying factor of around 2–3. Due to space restrictions, we can not give the transition identifications for all the lines in the current

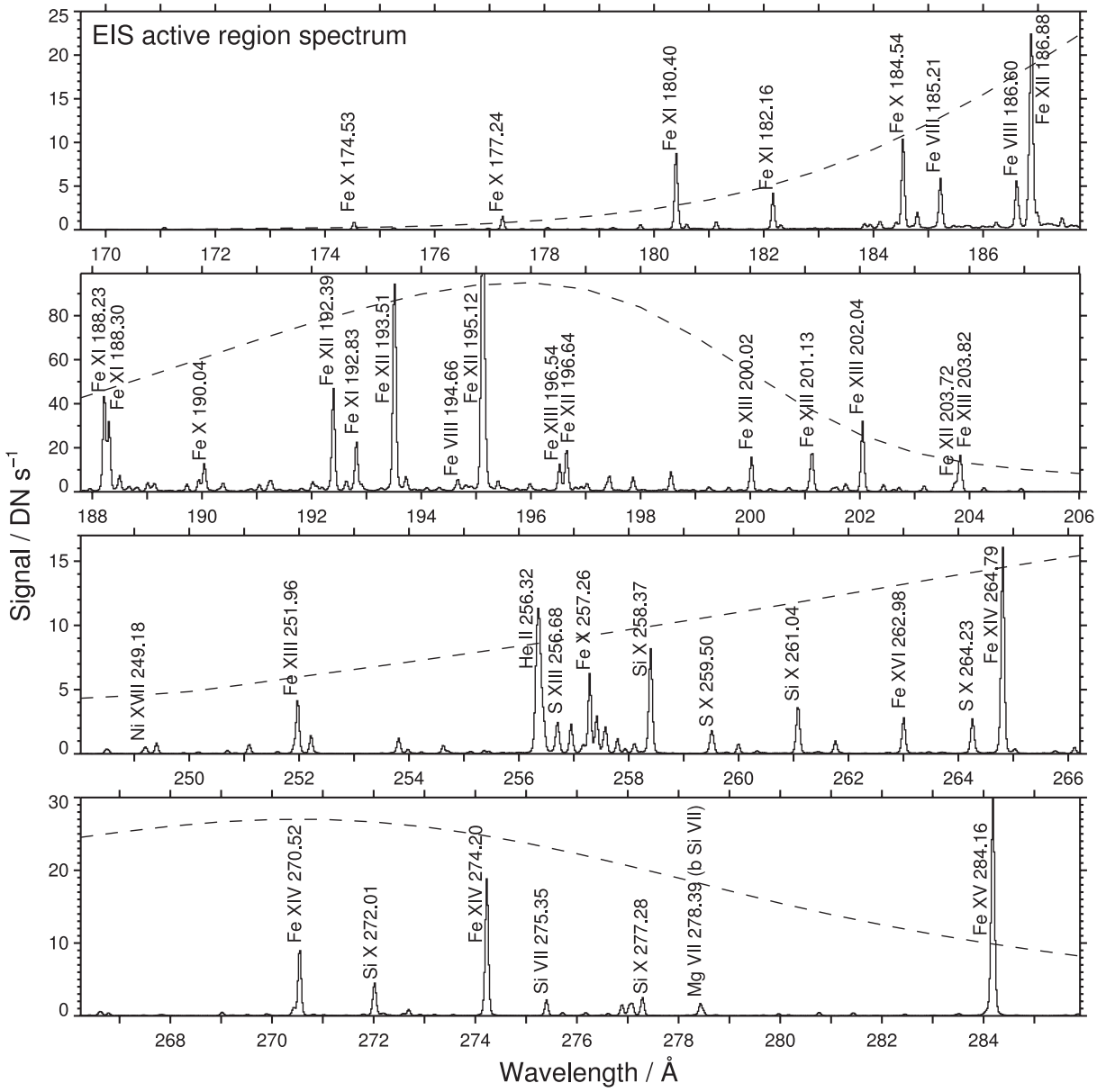

Fig. 2. EIS active region spectrum obtained on 2006 November 4 with identifications of important lines shown. The dashed line shows the effective area of the instrument, which has a peak value of 0.31 cm^2 in the SW band and 0.11 cm^2 in the LW band.

document. For these we refer the reader to Del Zanna and Mason (2005a) or the CHIANTI database.

3. Iron Lines

3.1. Fe VIII

All Fe VIII lines are found in the SW band, and the strongest lines are at 185.21, 186.60, and 194.66 Å lines, which are all comparable in strength in terms of DN. λ185.21 is blended with the Ni XVI 185.23 Å ($\log T = 6.4$) line which becomes apparent in active region intensity maps with a "mist" of emission visible around the hot core of the active region. The Ni XVI contribution can be estimated by observing the Ni XVI 195.27 Å line (which lies very close to Fe XII λ195.12) as the λ195.28/λ185.23 intensity has a fixed value of 0.23. λ186.60 is blended with Ca XIV λ186.61 ($\log T = 6.5$), and the Ca XIV contribution can be estimated by measuring the λ193.86 line: the λ186.61/λ193.86 intensity ratio being fixed at 0.69. Note that Fe VIII is typically found to be strongest in the footpoints of loops at the edges of active regions, where hot ions such as Ni XVI and Ca XIV are often negligible.

Fe VIII λ194.66 is not directly blended but has an unidentified line in the long wavelength wing at $\approx$ 194.80 Å. λ194.66 may possibly be affected if the Fe XII λ195.12 line shows a high velocity blue-shifted component, or is broadened significantly. In summary, we thus recommend observing both the λ185.21 and λ194.66 lines — the former is in a relatively clean part of the spectrum (apart from the high temperature Ni XVI line) making it good for velocity studies, and the latter can be used in active regions when Ni XVI significantly

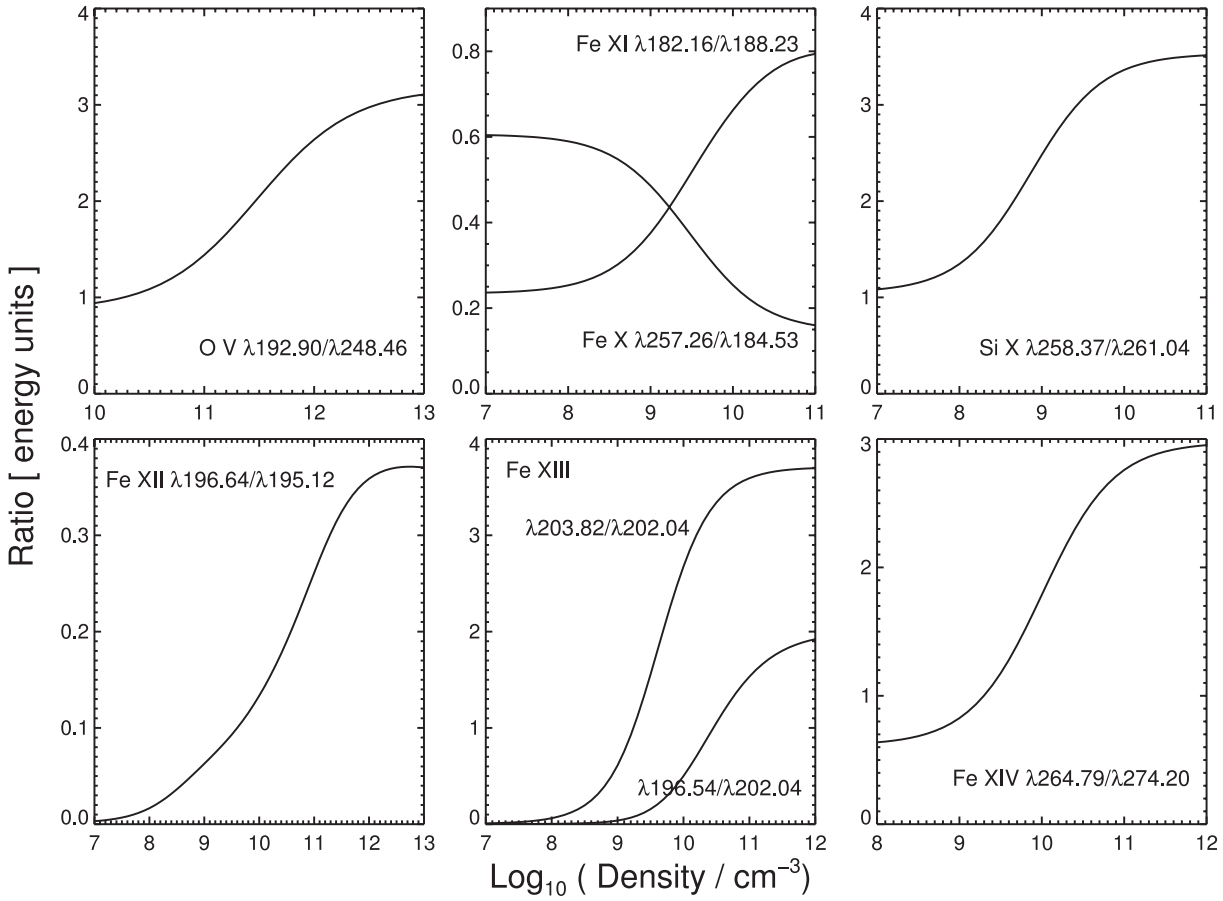

Fig. 3. Recommended density diagnostic emission line ratios discussed in the text. Plots derived using atomic data and software from v.5.2 of the CHIANTI atomic database. Note that the other recommended diagnostic — Mg VII λ280.78/λ278.39 — is presented in Young et al. (2007).

contaminates the λ185.21 line. The Fe VIII lines show density sensitivity below 10^8 cm^{-3} and so are not generally useful; the λ186.60/λ185.21 ratio is the best diagnostic in these conditions, however.

An important point to note about Fe VIII is that it seems to be formed at $\log T = 5.8$ rather than the temperature of $\log T = 5.6$ predicted by Mazzotta et al. (1998). This is discussed further in Young et al. (2007).

3.2. *Fe X*

The strongest Fe X lines observed by EIS are at 184.54, 190.04, and 257.26 Å (the latter actually a self-blend of two lines). λ184.54 and λ190.04 are comparable in strength in terms of DN. λ190.04 is partly blended with an unknown line at around 189.94 Å which seems to be formed around $\log T = 5.8$–5.9. The λ190.04/λ184.54 ratio is insensitive to density, but λ257.26 is sensitive to density when taken relative to either λ190.04 or λ184.54. The λ257.26/λ184.54 ratio is recommended and shown in figure 3. λ257.26 is in a crowded part of the spectrum and a large wavelength window (at least 50 pixels) is required to obtain a good estimate of the spectrum background.

3.3. *Fe XI*

Fe XI is a very complex ion and even line identifications of strong lines are uncertain. Improvements in computing power and techniques should yield accurate atomic data in the near future, and work is underway by P. J. Storey in collaboration with some of the present authors.

The strongest Fe XI lines observed by EIS are partly blended with each other and found at 188.23 and 188.30 Å. Although the identification of λ188.30 is uncertain, the λ188.23/λ188.30 ratio is found to be nearly constant in the EIS data with a ratio of around 0.7, suggesting they are from the same ion. We believe the $3s^2 3p^4\ ^3P_{2,1} - 3s^2 3p^3(^2D)3d\ ^3P^o_2$ transitions give rise to λ188.23 and another line at 192.83 Å, respectively. This latter line provides a component to the complex blend at this wavelength which is discussed further in subsections 4.2 and 7.4.

The Fe XI lines at 180.40 and 182.16 Å are well identified and density sensitive relative to each other, but the EA is low in this region. The λ182.16/λ188.23 density sensitive ratio is preferred (figure 3), with the proviso that the λ188.23 transition identification is uncertain.

3.4. *Fe XII*

Many discrepancies between theory and observations for Fe XII have been resolved recently following a new atomic

calculation (Del Zanna & Mason 2005b; Storey et al. 2005), and we can now have confidence in using the ion for diagnostic work.

The three strongest Fe XII lines are the decays of the $3s^2 3p^2(^3P)3d\ ^4P_{5/2,3/2,1/2}$ states to the ground state, giving lines at 195.12, 193.51, 192.39 Å, respectively. λ195.12 lies at the peak of the EIS sensitivity curve and so is the strongest emission line observed by EIS in most conditions. It is one of the EIS core lines and therefore included in all EIS studies. λ195.12 has been found to be broader than the λ193.51 line which could be indirect confirmation of the identification proposed in Del Zanna and Mason (2005b) of a Fe XII line at 195.18 Å. At 10^{10} cm^{-3} this line is predicted to contribute 10% to the feature at 195.1 Å.

The only problem with observing the λ195.12 line is that it is likely to saturate on the detector if long exposure times are used. In active conditions even a 30 s exposure can lead to saturation in bright parts of an active region. We thus recommend that the λ192.39 or λ193.51 lines are observed in addition to λ195 as they are around 27% and 60% weaker in terms of DN.

Fe XII provides some of the best density diagnostics for EIS. The ratio of either of the λ196.64 or λ186.88 lines to any of λλ195.12, 193.51, 192.39 is sensitive to a wide range of densities ($\log N_e = 8$–12). λ186.88 is a blend of two Fe XII lines, and is stronger than λ196.64 in terms of DN, but it is also blended with a S XI transition at 186.84 Å. This generally makes a small contribution to the Fe XII line, and it can be accurately assessed by measuring S XI λ191.27 as λ186.84/λ191.27 has a fixed ratio of 0.20. λ196.64 lies close to Fe XIII λ196.54 (another recommended line — see below) but can generally be resolved, and thus we recommend this line for the Fe XII density diagnostic (figure 3).

3.5. *Fe XIII*

The three most important Fe XIII lines are at 196.54, 202.04, and 203.82 Å. They form the best coronal density diagnostics available to EIS due to their high sensitivity to density (figure 3). λ203.82 is a blend of two Fe XIII lines at 203.80 and 203.83 Å that are approximately in the ratio 1:3. Interpretation of λ203.82 is hampered by a blend with Fe XII λ203.72, but fitting the combined feature with two Gaussians can usually separate the Fe XII and Fe XIII components. The λ202.04 line is unblended, while λ196.54 is easily resolvable from Fe XII λ196.64 in most conditions. The λ196.54/λ202.04 ratio is more sensitive to density than λ203.82/λ202.04 above around 10^{10} cm^{-3} and is also sensitive to higher densities, but both are highly recommended to be included in EIS studies.

Other strong Fe XIII lines are found at 197.43 Å, 201.13 Å (blended with Fe XII λ201.14), and 251.96 Å, but these are not as useful as the aforementioned lines.

3.6. *Fe XIV*

A number of prominent Fe XIV lines are found in the EIS wavebands, and the one recommended here is at 274.20 Å. Although there is a blend with Si VII λ274.18, this can be quantified if Si VII λ275.35 (one of the recommended lines) is also observed since the λ274.18/λ275.35 ratio is at most 0.25. In most active region conditions the blend can safely be ignored. The Fe XIV λ264.79 line yields a good density diagnostic relative to λ274.20 (figure 3) and is recommended for probing hotter parts of active regions. Another strong line is λ270.52, but this is weaker than λ274.20 in all conditions, and the λ264.79/λ270.52 ratio is less sensitive to density.

3.7. *Fe XV*

The Fe XV 284.16 Å line dominates this region of the EIS spectrum in active conditions and is the strongest line from the ion. We recommend its inclusion in any EIS study. Note that in quiet Sun conditions the line is very weak or non-existent and an Al IX line at 284.03 Å becomes apparent.

3.8. *Fe XVI*

Three lines are found in the EIS long wavelength band at 251.06, 262.98, and 265.00 Å. They are all temperature and density insensitive relative to each other, λ262.98 being the strongest. This latter line is unblended and is recommended for inclusion in all observations.

3.9. *Fe XVII*

Fe XVII is formed over a broad range of temperatures, with its maximum abundance at $\log T = 6.6$. The strongest Fe XVII transitions are found at X-ray wavelengths but there are a number of weak transitions in the EIS bands, particularly the LW band. The strongest of the lines is at 254.87 Å and, although it is much weaker than Ca XVII λ192.82 (which is formed at a similar temperature), it does not suffer the blending problems of this line. Note that v.5.2 of CHIANTI does not give the correct wavelength for this transition, instead listing it at 254.35 Å. The Fe XVII model is being reassessed by the CHIANTI team, and caution should be applied if using this line for quantitative analysis.

3.10. *Fe XXIII*

The λ263.76 line is predicted to be the strongest line during large flares, after the Fe XXIV lines, and should be unblended. All EIS studies for active regions, microflares, and flares are recommended to include this line.

3.11. *Fe XXIV*

The Li-like doublet $2s\ ^2S_{1/2}$–$2p\ ^2P^o_{3/2,1/2}$ gives rise to lines at 192.03 and 255.11 Å, respectively, and during large flares they become the most prominent lines in the EIS spectra. λ192.03 is blended with another line, believed to be from Fe XI, while λ255.11 is blended with a relatively weak S X line at 255.06 Å ($\log T = 6.1$), thus care must be taken when searching for a weak signal in the Fe XXIV lines. Although the intensity of λ192.03 is predicted to be 2.5 times stronger than λ255.11, it will be around 12 times stronger in terms of DN due to the larger EA at 192 Å. Note that the Fe XXIV lines have been seen in observations of C class flares by EIS, and are recommended for all active region studies.

4. Oxygen Lines

O IV–VI each have very strong 2s–2p transitions at longer UV wavelengths, beyond the reach of EIS. However, these ions have a number of weak $n = 2$ to $n = 3$ transitions in the

EIS wavebands that are valuable diagnostics of the transition region.

4.1. O IV

There are many weak lines from O IV predicted in the SW and LW bands. The strongest is found at 279.93 Å, and there is a nearby line at 279.63 Å that is a factor 2 weaker. These O IV lines are weaker than the lines of O V and O VI mentioned below, and so the latter are generally preferred unless the transition region is specifically the region of interest.

4.2. O V

The strongest O V lines arise from the $2p\,^3P^o_J$–$3d\,^3D_{J'}$ multiplet and are found between 192.75 and 192.91 Å, contributing to one of the most difficult parts of the EIS spectrum to analyse. The EIS core line Ca XVII λ192.82 ($\log T = 6.7$) is in this region, as well as Fe XI λ192.83. There are six O V transitions in all from the multiplet, although one has negligible intensity. The remaining five lines give rise to three features at 192.75 Å, 192.80 Å, and 192.90 Å (the latter two comprising of two co-incident transitions each). There is density sensitivity amongst the lines, but they lie in the approximate ratio 0.16 : 0.4–0.45 : 1.0 in most conditions — see Young et al. (2007). λ192.80 is blended with the Fe XI and Ca XVII lines, with λ192.75 discernible in the SW wing. The λ192.90 component can usually be resolved and thus by measuring this line one can estimate the O V contribution to the Fe XI–Ca XVII feature.

The other useful O V line is at 248.46 Å which is around ten times weaker than the λ192.90 line due to the much lower EA at this wavelength. The λ192.90/λ248.46 ratio is sensitive to densities above 10^{10} cm^{-3} (figure 3) and thus will be useful for the study of the active region transition region brightenings discussed by Young et al. (2007). CHIANTI lists a blend with Al VIII λ248.46 ($\log T = 6.0$) which should only be a minor component in most conditions. However, its contribution can be estimated from the Al VIII λ248.46/λ250.14 intensity ratio which has a fixed value of 0.60.

4.3. O VI

Two O VI lines are available at 183.94 and 184.12 Å and the ratio λ183.94/λ184.12 is 0.5. They lie close to the recommended line Fe X λ184.54 and a single broad wavelength window can be used to pick up all three lines.

5. Magnesium Lines

5.1. Mg V

Only one line is found in the EIS wavelength bands at 276.58 Å. While very weak in most circumstances, the line is significantly enhanced in loop footpoints (Young et al. 2007) and gives valuable temperature information.

5.2. Mg VI

Two lines are found at 268.99 and 270.39 Å which are in the approximate ratio of 1:2 in most conditions. λ270.39 lies in the wing of Fe XIV λ270.52 which is usually much stronger in active region conditions. λ268.99 is unblended. Both lines can be strongly enhanced in loop footpoints as demonstrated in Young et al. (2007). Note that λ268.99 is relatively isolated and thus valuable for identifying loop footpoints in 40″ slot data.

5.3. Mg VII

The $2s^22p^2\ ^3P_J$–$2s2p^3\ ^3S^o_1$ multiplet is found at 276.14, 276.99, and 278.39 Å, with the lines lying in the ratio 0.20 : 0.60 : 1.0. The strongest line, λ278.39, is blended with Si VII λ278.44 but they can be resolved either through a double Gaussian fit, or by using the Si VII λ278.44/λ275.35 insensitive ratio (Young et al. 2007). λ276.99 is blended with Si VIII λ277.04, but λ276.14 is unblended. A further Mg VII line is found at 280.75 Å which is unblended and of great value as a density diagnostic relative to any of the other three lines, being sensitive in the range 10^8–10^{11} cm^{-3}. The ratio is used by Young et al. (2007) to measure the density in loop footpoints.

6. Silicon Lines

6.1. Si VII

The six $2s^22p^4\ ^3P_J$–$2s2p^5\ ^3P^o_{J'}$ transitions are found in the EIS LW band, and the strongest is at 275.35 Å which is unblended. Note that, from visual inspection of EIS images, Si VII is formed at around the same temperature as Fe VIII but is weaker by a factor two in terms of DN compared to the strongest lines from that ion.

6.2. Si X

The six lines belonging to the $2s^22p\ ^2P^o_J$–$2s2p^2\ ^2P_{J'}$ and $2s^22p\ ^2P^o_J$–$2s2p^2\ ^2S_{1/2}$ transitions are found in the LW band, with the strongest being λ258.37 and λ261.04 which form a density diagnostic (figure 3). Both lines appear to be unblended. Si X λ256.37 is blended with He II λ256.32, hampering interpretation of this key line, however the λ256.37/λ261.04 ratio has a fixed intensity ratio of 0.89, allowing the Si X contribution to be estimated.

According to the Mazzotta et al. (1998) ion balance calculations, Si X is formed at almost exactly the same temperature as Fe XII, and so the λ258.37/λ261.04 density diagnostic should probe the same region as Fe XII λ196.64/λ195.12. Although Fe XII λ196.64 has approximately the same DN as Si X λ258.37, Fe XII λ195.12 is much stronger than Si X λ261.04 and so the Fe XII ratio is to be preferred.

7. Other Ions

7.1. He II

He II λ256.32 is the coolest line observed by EIS and also the strongest line formed below 10^6 K, so it was selected as one of the three EIS core lines to appear in every EIS study. It is actually a self blend of two transitions with almost identical wavelengths. Interpretation of λ256.32 is complicated by blends with Si X λ256.37 (see subsection 6.2), Fe XIII λ256.42, and Fe XII λ256.41. For disk observations of the quiet Sun and active regions, He II should dominate the feature contributing 80% or more to the blend, but above the limb the coronal lines will generally dominate. If the He II line is crucial to your science then we recommend taking other Si X, Fe XII, and Fe XIII lines in order to correctly estimate their contributions.

Despite these blends, λ256.32 is still very useful for the study of explosive events and other dynamic phenomena.

7.2. S XIII

The strongest line of the S XIII spectrum is found at 256.68 Å and is comparable in strength to Fe XVI λ262.98 which is formed at the same temperature. There is a contribution from Ni XVI λ256.62, but this can be estimated from the λ256.62/λ195.28 intensity ratio which is approximately 0.28 in all conditions. The S XIII line is also close to He II λ256.32 and so can be affected if the latter is broadened or redshifted in dynamic events.

7.3. Ni XVII

The λ249.18 line of Ni XVII is the analogous transition to λ284.16 of the iso-electronic Fe XV ion. The line is unblended and a valuable probe of the hot cores of active regions. It is weaker than Fe XVI λ262.98 and S XIII λ256.68, but according to the Mazzotta et al. (1998) ion balance calculations this line should be formed in slightly hotter plasma, in the $\log T = 6.4$–6.5 range.

7.4. Ca XVII

Ca XVII is formed at $\log T = 6.7$ and its strongest line is found in the EIS SW band at 192.82 Å, where the instrument is very sensitive. This line was selected as one of the three EIS core lines to ensure at least one flare line is present in all EIS studies. However, λ192.82 is part of a complex blend comprising five lines of O V and two lines of Fe XI and so requires careful analysis. The O V lines were discussed in subsection 4.2 where a method of estimating the contribution from O V was given.

Using CHIANTI to estimate the contribution of Fe XI is somewhat uncertain due to the known problems with line identifications and atomic data for this ion. There are two lines given by CHIANTI at wavelengths 192.830 and 192.832 Å. The latter is a theoretical wavelength and thus uncertain. λ192.830 has a fixed ratio relative to the strong λ188.23 line (subsection 3.3), with a theoretical intensity ratio of 0.21. λ192.832 is predicted to be weaker than λ192.830, the ratio λ192.832/λ192.830 varying from 0.20 at low density to 0.55 at high density. Inspecting EIS spectra taken above the solar limb in quiet Sun conditions (where both O V and Ca XVII are negligible), we find the observed λ192.83/λ188.23 ratio to be around 0.26, which is consistent with both the CHIANTI λ192.830 and λ192.832 lines contributing to the observed feature at 192.83 Å. Our recommended prescription for estimating the Fe XI contribution to the Ca XVII line is thus to measure the Fe XI λ188.23 line and multiply the intensity by the factor 0.26 to obtain the λ192.83 intensity.

Despite the difficulties with blending it should be noted that Ca XVII completely dominates the other lines in large flares and thus is an important line for such observations.

8. Considerations for Designing EIS Observing Studies

Table 1 summarises the emission lines recommended in the previous sections. Each ion in the Sun's atmosphere is formed over a characteristic narrow temperature range, and the temperature of maximum abundance ($T_{\max}$) is given in table 1. The recommended density diagnostics described in the text are summarised in figure 3. The data rate for EIS is sufficiently high that 10–20 wavelength windows can be chosen in most cases and thus many of the recommended lines can be selected. For density diagnostics, we recommend the Fe XII λ196.64/λ195.12, and Fe XIII λ196.54/λ202.04 and λ203.82/λ202.04 ratios for all studies. For the other diagnostics an assessment should be made based on the science to be achieved (e.g., for transition region brightenings in active regions the O V and Mg VII ratios should be selected). The EIS planning software allows spectral windows to have variable sizes which can be used to select windows that span more than one emission line. This is useful for lines that are close in wavelength (e.g., Fe VIII λ194.66 and Fe XII λ195.12) and for cases where a large window is required to yield a good background measurement (e.g., Fe X λ257.26).

Although the EIS emission lines typically extend over 12 wavelength pixels we recommend setting the widths of wavelength windows to be 32 or 40 pixels (window sizes have to be multiples of 8 pixels) as the emission lines have been seen to broaden significantly in flares and other dynamic

Table 1. EIS emission lines recommended to be included in observation studies. A "b" indicates blending (see text).

Ion	Wavelength (Å)	$\log T_{\max}$
Cool lines ($\log T_{\max} < 6.0$)		
He II	256.32 b	4.7
O V	192.90	5.4
	248.46 b	5.4
O VI	184.12	5.5
Mg V	276.58	5.5
Mg VI	268.99	5.7
Mg VII	278.39 b	5.8
	280.75	5.8
Si VII	275.35	5.8
Fe VIII	185.21	5.8
	194.66	5.8
Coronal lines ($6.0 \leq \log T_{\max} < 6.4$)		
Fe X	184.54	6.0
	257.26	6.0
Fe XI	188.23	6.1
	182.16	6.1
Si X	258.37	6.1
	261.04	6.1
Fe XII	195.12	6.1
	196.64	6.1
Fe XIII	196.54	6.2
	202.04	6.2
	203.82	6.2
Fe XIV	274.20 b	6.3
	264.79	6.3
Fe XV	284.16	6.3
Hot lines ($6.4 \leq \log T_{\max} < 6.7$)		
S XIII	256.68 b	6.4
Fe XVI	262.98	6.4
Ni XVII	249.18	6.5
Fe XVII	254.87	6.6
Flare lines ($\log T_{\max} \geq 6.7$)		
Ca XVII	192.82 b	6.7
Fe XXIII	263.76	7.1
Fe XXIV	192.03 b	7.2
Fe XXIV	255.11 b	7.2

phenomena. Broad windows also allow the background level in the spectra to be more accurately measured. If high cadence is required, then using 24 pixels to reduce the data rate is acceptable, but high velocity events may be missed. For Fe XII λ195.12 a window size of 48 pixels (or larger) is recommended as the instrument is so sensitive at this wavelength.

The choice of exposure time for EIS studies depends on both the target and science objective. If good signal is required in a wide range of lines, then exposure times of 60–90 s for quiet Sun and 20–40 s for active regions are recommended. If higher cadence is required, then good signal in the strong lines (including the recommended Fe XII and Fe XIII density diagnostics) can be obtained in 20 s for quiet Sun and 5 s for active regions. Exposure times down to 1 s will give a good signal in the Fe XII λ195.12 line in active regions. These exposure times are for the 1″ slit — they should be reduced by a factor 2 for the 2″ slit, and about a factor 2.5 for the slots.

9. Summary

The quality of the EIS spectra are outstanding and reveal a large number of emission lines throughout the two wavelength bands that offer exciting diagnostic opportunities, a number of which are exploited in papers in this volume of PASJ. The present work has summarised some of the key emission lines and density diagnostics based on evaluations of the initial EIS data-sets using the CHIANTI atomic database. It is hoped that this will be a valuable reference for scientists designing EIS studies, and help improve the science return from the instrument.

Hinode is a Japanese mission developed and launched by ISAS/JAXA, with NAOJ as domestic partner and NASA and STFC (UK) as international partners. It is operated by these agencies in co-operation with ESA and NSC (Norway). G. Del Zanna and H. E. Mason acknowledge support from PPARC/STFC. The work of E. Landi is supported by NASA. G. Del Zanna thanks the hospitality of DAMTP, University of Cambridge.

References

Culhane, J. L., et al. 2007, Sol. Phys., 243, 19
Del Zanna, G., & Mason, H. E. 2005a, Adv. Space Res., 36, 1503
Del Zanna, G., & Mason, H. E. 2005b, A&A, 433, 731
Dere, K. P., Landi, E., Mason, H. E., Monsignori Fossi, B. C., & Young, P. R. 1997, A&AS, 125, 149
Kosugi, T., et al. 2007, Solar Phys., 243, 3
Landi, E., Del Zanna, G., Young, P. R., Dere, K. P., Mason, H. E., & Landini, M. 2006, ApJS, 162, 261
Malinovsky, M., & Heroux, L. 1973, ApJ, 181, 1009
Mazzotta, P., Mazzitelli, G., Colafrancesco, S., & Vittorio, N. 1998, A&AS, 133, 403
Storey, P. J., Del Zanna, G., Mason, H. E., & Zeippen, C. 2005. A&A, 433, 717
Young, P. R., Del Zanna, G., Mason, H. E., Doschek, G. A., Culhane, J. L., & Hara, H. 2007, PASJ , 59, S727